Accepted Manuscript

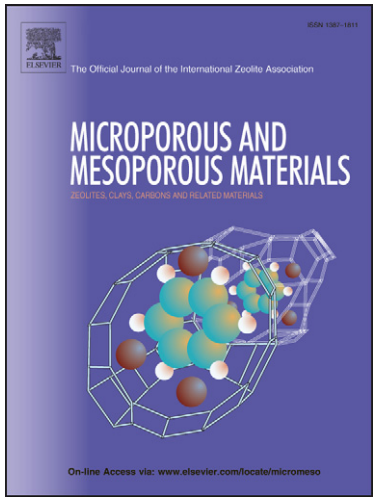

The role of different parameters of synthesis in the final structure of Ti containing mesoporous materials

Griselda A. Eimer, Corina M. Chanquia, Karim Sapag, Eduardo R. Herrero

PII: S1387-1811(08)00276-X
DOI: 10.1016/j.micromeso.2008.05.040
Reference: MICMAT 3763

To appear in: *Microporous and Mesoporous Materials*

Received Date: 10 April 2008
Revised Date: 21 May 2008
Accepted Date: 28 May 2008

Please cite this article as: G.A. Eimer, C.M. Chanquia, K. Sapag, E.R. Herrero, The role of different parameters of synthesis in the final structure of Ti containing mesoporous materials, *Microporous and Mesoporous Materials* (2008), doi: 10.1016/j.micromeso.2008.05.040

The role of different parameters of synthesis in the final structure of Ti containing mesoporous materials

Griselda A. Eimer*[1], Corina M. Chanquia[1], Karim Sapag[2], Eduardo R. Herrero[1]

[1]Centro de Investigación y Tecnología Química (*CITeQ*)), Universidad Tecnológica Nacional, Facultad Regional Córdoba, Maestro Lopez esq. Cruz Roja Argentina (5016) Córdoba, Argentina. *E-mail: geimer@scdt.frc.utn.edu.ar

[2] Instituto de Física Aplicada -CONICET, Universidad Nacional de San Luis, Chacabuco 917, 5700 San Luis, Argentina.

Abstract

Ti-containing mesoporous materials have been prepared by hydrothermal synthesis at 373 K and compared to pure siliceous MCM-41 synthesized in the same conditions. A detailed and correlative study about the effect of different synthesis parameters on the physicochemical properties of the material has been carried out. All the samples showed typical XRD patterns of a kind MCM-41 structure. It seems that the synthesis time and the surfactant chain length are critical variables to obtain good structures. Mesoporous structure allowed the incorporation of different degrees of Ti loading, although a lower degree of ordering was observed with the increase of metal content above 1%. Moreover, a high incorporation of Ti into the structure seems responsible for the development of a secondary mesoporosity confirmed by TEM and associated with a pronounced hysteresis loop in the N_2 isotherm. DRUVA-Vis and XPS studies revealed that the Ti species are mainly found isolated and tetrahedral coordinated into the framework. The superego-Ti(IV) species generated by the interaction of Ti-MCM-41 with aqueous H_2O_2 have been studied by EPR spectroscopy and correlated to DRUVA-Vis and XPS measurements.

Keywords: Ti-MCM-41; mesoporous materials; M41S; titanium; physicochemical properties

1. Introduction

The ever-growing importance of the inorganic materials with controlled pore size distribution is mainly due not barely to the deep theoretical interest on such compounds, but also to the wide number of applications in which they are used (not only in catalysis) [1]. The major success in this subject has been the synthesis of a series of well defined mesoporous molecular sieves called M41S [2-4] which possess pore diameters ranging from 2 to 10 nm and large and accessible internal areas (higher than 1000 m^2/g). Instead of using single molecules as templates, like in the case of microporous zeolite synthesis, Chemists from Mobil utilized ordered long-range supramolecular aggregates of surfactant micelle molecules. By varying the chain length of the surfactant templates, it is possible to synthesize such mesoporous molecular sieves in a wide range of pore sizes [5] which fill the gap in catalytic chemistry between the crystalline microporous zeolites and amorphous disordered mesoporous supports, like silica gel. MCM-41, the member of the M41S family which possesses a hexagonal arrangement of uniformly sized mono-dimensional pores, has been the most widely studied. These materials opened an interesting field of applied research thanks to the several potential applications in the pharmaceutical and fine chemical industries, petroleum refining, adsorption and separation processes and heterocatalysis, mostly due to their large surface area and controlled pore dimensions with uniform pore size distribution [6-13]. A very interesting characteristic of these materials is that their large and accessible internal surface may contain several types of active sites: Lewis and Bronsted acids, transition metal ions, nanometric metal clusters. Many elements of the periodic table can be incorporated into the network or easily exchanged in extra-framework positions. The introduction of transition metals such as titanium, chromium

and vanadium is very important from the point of view of the preparation of mesoporous catalysts with redox properties. In particular, molecular sieves containing a transition metal cation, Ti^{+4}, in framework positions have a very good activity in shape selective oxidation - reduction reactions especially of bulky molecules, showing a great potential in the fine chemicals industry [14-17]. Although there are many reports concerning the synthesis and characterization of Ti-MCM-41 materials, the influence of different synthesis variables on the structural properties and the chemical environment around the Ti atoms continues under discussion. Thus, because the rates of polymerization of the silicium and titanium species are different, the aging time of the synthesis result an important parameter that can change the physico-chemical properties of the final solid. Moreover, different Ti loadings in the catalyst may induce changes not only in the textural characteristics but also in the surface chemical properties of the material. In this work we study the influence of several synthesis parameters on the structural, textural and chemical properties of Ti-containing MCM-41 catalysts. In particular, the role of the Ti incorporation on the presence of an unusual nitrogen isotherm and intra-crystalline porosity was also discussed. On the other hand, it is known that the Ti species in MCM-41 framework positions are the active sites for carrying out selective catalytic oxidations of hydrocarbons using peroxides as oxidants. Moreover, TiO_2 crystals with an anatase structure in the titanosilicates were proved to lower the catalytic performance by enhancing the decomposition of H_2O_2 into water and oxygen. Therefore, it becomes very crucial to control the synthesis parameters in order to obtain anatase-free titanosilicates with high structure quality, maximizing the presence of isolated framework Ti species. The catalytic performance of these materials in the oxidation of cyclohexene with H_2O_2 has been reported by us in reference 18. Here, the nature of the framework Ti sites and of the reactive oxo-species (oxo-titanium) generated over these titanosilicates during oxidation with H_2O_2 has been

investigated by electron paramagnetic resonance spectroscopy (EPR) and correlated to DRUVA-Vis and XPS results.

2. Experimental

Catalyst Preparation

The titanium-containing mesoporous materials were prepared by hydrothermal synthesis using dodecyltrimethyl ammonium bromide (DTMABr) or cetyltrimethyl ammonium bromide (CTMABr) as a template. Tetraethoxysilane (TEOS) and titanium isopropoxide (TIP) were used as the Si and Ti sources, respectively. The catalysts were synthesized from gel of molar composition: Si/Ti= 20-180, OH/Si= 0.30, surfactant/Si= 0.4, water/Si= 60. In a typical synthesis, TEOS (Fluka≈ 98 %) and TIP (Fluka≈98 %) were vigorously mixed for 30 min. Then, 25 wt.% solution of DTMABr or CTMABr (Fluka≈98 %) in ethanol and 70 % of the tetraethylammonium hydroxide 20 wt.% aqueous solution (TEAOH) (Fluka) were added drop wise under stirring which was continued during 3 h. Finally, the remaining TEAOH and the water were added drop wise to the milky solution which was then heated at 353 K for 30 min to remove both the ethanol used in the solution and the additional produced in the hydrolysis of TEOS. The pH of the resultant gel was 11.5. This gel was transferred into Teflon-lined stainless-steel autoclave and kept in an oven at 373 K for 0-7 days under autogeneous pressure. The solid was then filtered off, washed with distilled water and dried at 333 K overnight. To remove the template, the samples were heated (heating rate of 2 °C/min) under N_2 flow up to 773 K maintaining this temperature for 6 h and subsequently calcined at 773 K under air flow for 6 h. For comparison purposes, a pure siliceous MCM-41 sample was prepared by the same synthesis method.

Physicochemical characterization

The titanium content in the final solid products was determined by inductively coupled plasma atomic emission spectroscopy (ICP-AES) in a VGelemental Plasma Quad 3 mass spectrometer. Calcined samples were previously dissolved and digested in a mixture of H_2SO_4-HF (3:1). The resulting solution was diluted and was ready for the ICP-AES measurement. X-ray powder diffraction patterns were collected in air on a Rigaku diffractometer at room temperature using CuKα radiation of wavelength 0.15418 nm. Diffraction data were recorded between 1-40° at an interval of 0.01° and a scanning speed of 2° per minute. Diffuse reflectance UVA-vis spectra were recorded using an Optronicss OL 750-427 spectrometer in the wavelength range 200-500 nm. The specific surface area, the pore size distribution and the total pore volume were determined by N_2 adsorption-desorption isotherms obtained at 77 K using Micromeritics ASAP 2010 equipment. The surface area was calculated by the BET method in the range p/p_0 0.01-0.25. The total pore volume (V_p) was calculated by Gurvitsch rule. Density Functional Theory method (DFT) was applied to evaluate the pore size distribution since this method, based on molecular statistical approach, is applied over the complete range of the isotherm and is not restricted to a confined range of relative pressures or pore sizes [19]. For the transmission electron microscopy (TEM) experiments, the samples were crushed, dispersed in acetone and dropped on a holey carbon grid. Micrographs were recorded using a JEOL JEM 2000FX microscope operating at 200 kV equipped with an Oxford X-ray detector. X-ray photoelectron spectra (XPS) were acquired with a VG Escalab 200R spectrometer equipped with a hemispherical electron analyzer and a Mg Kα (hυ = 1253.6 eV) X-ray source. The sample was first placed in a small stainless-steel holder mounted on a sample-rod in the pretreatment chamber of the spectrometer, and then degassed at room temperature and 10^{-5} mbar for 5 h prior to transfer to the analysis chamber. Residual pressure was maintained below 3 x 10^{-8} mbar. The binding energies (BE) were referenced to the C 1s

peak (284.9 eV) to account for the charging effects. EPR spectra were measured at 107, 220 and 295 K using a Bruker ESP 300 spectrometer operating at X band frequency and 9.5 GHz field modulation. Before taking EPR measurements, the samples were activated in air at 373 K. In the experiments with H_2O_2, a defined amount of the solvent (acetonitrile, 0.5 mL) was added to a specific amount of Ti-MCM-41 sample (55mg), such that the catalyst was completely saturated in the solvent. Then 0.15 mL of aqueous H_2O_2 (30 wt. %) was added. After the addition of H_2O_2, the color of the solid changed from white to yellow rapidly.

3. Results and Discussion

Figure 1 presents the XRD patterns of calcined samples prepared using DTMABr and CTMABr as templates with a Si/Ti molar ratio of 60 in the synthesis gel and 3 days of hydrothermal treatment. Both samples exhibit an intense low-angle reflection at approximately 2.5-3.0°, characteristic of mesoporous materials. Even though both samples showed specific surface areas about 1500 m^2/g, the mesostructure obtained with DTMABr exhibit, besides the main peak, two weak peaks ascribed to (110) and (200) reflections, which is characteristic of a MCM-41 structure. On the other hand, the sample obtained with CTMABr under similar synthesis conditions exhibited a XRD pattern not enough defined which indicates a lower structural regularity. This feature suggests that the cooperative character of the electrostatics assembly mechanism of anionic inorganic species with a cationic surfactant (S^+I^-) could be affect by the alkyl chain length of the surfactant. For both samples, the structure was assumed to be MCM-41 type and the lattice parameter (a_0) was also calculated for comparative purposes.

Thus, as it was expected, this lattice parameter (a_0) increased from 36.28 Å to 44.40 Å by increasing the surfactant chain length.

Considering that the use of DTMABr allows obtaining a better pore ordering, we have chosen this surfactant as template in order to study the influence of other synthesis parameters on the mesostructures formed.

Figure 2 shows the ordering degree of the pore structure (structural regularity) of a calcined mesoporous sample synthesized with DTMABr as surfactant and molar ratio Si/Ti= 60, versus the reaction time. The ordering degree of the structure was evaluated against *internal standard* sample (hydrothermal treatment for 1 day) which was arbitrarily considered as *reference* (100% regularity) as it showed the better defined XRD pattern with the highest intensity for the (100) diffraction peak. As it can be observed, the mesostructure was formed even before the hydrothermal treatment. However, the structural regularity was increased when the sample was hydrotermally treated, being enough 1-3 days of synthesis to reach a good structure and a high surface area around 1600 m^2/g. On the other hand, it is remarkable that all the samples remained stable after calcination at 773 K.

Table 1 summarizes the chemical composition and physical properties of calcined Ti-MCM-41 type materials prepared with different Si/Ti molar ratios (DTMABr as template and 1 day of hydrothermal synthesis), together with those of the corresponding pure siliceous MCM-41 sample. The XRD patterns of these samples are shown in Figure 3. All the samples exhibit the main reflection peak at low angles (2θ = 2.5-2.8°). The pure siliceous material and the sample with the lowest Ti content exhibit, besides the sharp (100) reflection peak, the other peaks ascribed to (110) and (200) reflections, characteristic of a highly ordered MCM-41 structure. As the content of Ti increases, there is a decrease in the intensity of the first peak besides an evident broadening for all peaks, which can be attributed to a reduction in the long-range order

of the structure. On the other hand, all the samples show large surface areas above 1400 m^2/g and total pore volumes about 0.65-0.85 cm^3/g, which are typical of mesoporous materials. However, when the Ti content in the material increases the surface area decreases which is clearly correlated to the decrease in the structural order observed. Due to the differences in the ionic radio of Ti^{+4} (0.68 Å) and Si^{+4} (0.41 Å), the substitution of the larger Ti^{+4} ion in place of Si^{+4} invariably should distort the geometry around Ti from an ideal T_d. Therefore, the length of Ti-O-Si bond, different from that of Si-O-Si, should certainly lead to some structure deformation. Moreover, an increasing Ti content may obstruct the structure-directing action of the template by changing its ionic strength, hindering the formation of the tubular mesoporous structure. This could result in the formation of partially broken pores and consequently low surface areas and structural regularity. In addition, as the content of Ti is increased, the main XRD peak slightly shifts towards a lower diffraction angle and a slight increase in the parameter "a_0" and the pores size is detected (Table 1). Taking into account that the bond length of Ti-O-Si is longer than the Si-O-Si one, this feature may be consistent with the probable incorporation of Ti into the mesoporous framework [20]. On the other hand, no diffraction peaks in the region of higher angles (10-50°) could be observed suggesting the absence of a bulk anatase phase in the samples [21].

Figure 4 shows N_2 adsorption/desorption isotherms of these calcined samples prepared with different Si/Ti molar ratios. All the samples exhibit type IV isotherms typical of mesoporous structures with a sharp inflection at relative pressure (P/P_0) of 0.1-0.25 characteristic of capillary condensation inside the conventional mesopores present in MCM-41 structure (primary or structural mesopores). Such inflection provides also clear evidence for narrowly defined diameter range for mesoporous channels of these materials, as it can be seen in Figure 5. On the other hand, N_2 isotherm for the pure siliceous material was rather flat at relative pressures above the

capillary condensation pressure characteristic of primary mesopores. No hysteresis loop is present, indicating that no other mesopores than those corresponding to the mesoporous channels, characteristic of MCM-41 materials, were detected [22-24]. For sample Ti-MCM-41(180), a very small hysteresis loop, which is closed at $p/p_0 \sim 0.45$, is additionally observed in the isotherm. Meanwhile, the isotherms of the samples Ti-MCM-41(60) and Ti-MCM-41(20), synthesized with the highest Ti contents, show the presence of a pronounced hysteresis loop with a sharp decrease of the desorption branch at $p/p_0 \sim 0.45$-0.5. According to the references [22-24], this feature in these materials would be resulting from a capillary condensation in secondary mesopores. Indeed, it is noticeable how the increasing Ti content enhances the pore volume associated with the hysteresis loop ($0.4 < p/p_0 < 0.6$ in Table 1). Therefore, the titanium ion seems to be responsible for the apparition of the hysteresis having a specific role in the development of this secondary porosity.

According to some authors [25], the nonstructural porosity is consisting of large cavities eventually interconnected and accessible through necks which have an average diameter smaller than those of the main voids. Transmission electron microscopy studies of the calcined sample Ti-MCM-41(20) have been carried out in order to verify the presence of such cavities. TEM images of the sample are shown in Figure 6. It can be observed in the micrograph that regions of low contrast randomly interrupt the pores arrangement characteristic of the mesoporous material. Such weak regions can be attributed to the presence of cavities that permeate the entire bulk, giving rise to a secondary porosity [24].

Meanwhile the genesis of the secondary mesopores is not fully understood, I. Diaz et al. [24] have reported that a change in the micellar size might favor the change from cylindral micelles to more complex aggregates. These aggregates would be responsible for the building-up of such secondary porosity. As we mentioned above, a

great amount of Ti in the synthesis medium may interfere in the formation of the micelles by changing its ionic strength, giving rise to these complex aggregates.

DRUVA-Vis spectroscopy of all the calcined samples prepared with different Si/Ti molar ratios (DTMABr as template and 1 day of hydrothermal synthesis) (Figure 7) allowed us to confirm that, no segregated anatase phase is present [18,20,26-29]. Moreover, an intense DRUVA-Vis band at 210 nm in all the samples indicate that most of Ti species are isolated and in tetrahedral coordination inside the framework [18,20,26-29]. For the sample with the highest Ti content (Ti-MCM-41(20)), a shoulder at 250-290 nm was also observed, which can indicate the presence of partially polymerized Ti-O-Ti species in the framework probably originated by the higher rate of polymerization of TIP than the one of TEOS [18,20,27]. Such Ti-O-Ti clustering, as result of a probably incipient polymerization of Ti species, could be contributing to the lower structural ordering and surface area observed for this sample. Furthermore, the presence of higher coordinated Ti species probably due to the insertion of water molecules upon hydration should be also considered [18].

XPS analysis has been done in order to obtain additional information about the chemical nature of the active species present on the catalyst. Figure 8 shows the Ti 2p spectra for the Ti-MCM-41(20) sample. As it is evident from the curve-fitted spectra, the Ti 2p regions show two doublets with an energy separation of 1.5 - 2 eV that, according to references [30-32], may correspond to titanium in tetrahedral (higher BE, square labels) and octahedral (lower BE, rhombus labels) coordination. As it was mentioned above, the tetrahedral coordination is referred to titanium accommodated into the silica framework. According to the literature [32], the octahedral coordination may derive from conversion of tetracoordinated titanium located at the surface of the material to octahedrally coordinated titanium by reaction with H_2O (g) in the atmosphere as well as to segregation of TiO_2 species at the surface of the materials.

Taking into account that, for our sample, the presence of extra-framework TiO_2 has just been discarded by DRUVA-Vis, this higher Ti atoms coordination could be attributed both to water molecules adsorbed on the catalyst and to the formation of some Ti-O-Ti clustering in the framework (evidenced by DRUVA-Vis). As it can also be observed, the tetrahedral component (higher BE) is rather higher than octahedral component, corroborating that most of Ti species would be in isolated and tetrahedral positions in the framework.

Although the characterization of titanium in titanosilicates by EPR is limited due to the diamagnetic nature of the most common oxidation state of Ti (Ti^{+4}) , this technique is a powerful tool to elucidate the local structure of catalytically active species such as the oxo-titanium radical ions. The Ti sites in different structural environments can generate reactive oxygen species having different structures and reactivity. Thus, three types of oxo-titanium species (hydroperoxo-, peroxo- and superoxo-titanium) have been stated in the literature [33-36] as being generated by contacting titanosilicates with H_2O_2. Taking into account that the isolated tetrahedral Ti sites are the centers that can activate the H_2O_2 and yield these different oxo-Ti(IV) species, it is possible to conclude that the presence of any of these species can be attributed to framework Ti(IV) ions. Then, in order to corroborate the oxidation state and the coordination environment of the Ti and to infer about the nature of the reactive oxo-titanium species formed during the oxidation reactions with H_2O_2 over our Ti containing catalysts, EPR spectra were recorded before and after their interaction with H_2O_2. No EPR spectrum was observed for all the samples, revealing that all the titanium ions are present in the +4 oxidation state in the silicalite structure. On contact with 30% aqueous H_2O_2, the solid catalysts became yellow and exhibited three EPR signals, characteristic of a rhombic *g* tensor. Representative EPR spectra of a sample (Ti-MCM-41(20)) after its contact with aqueous H_2O_2, recorded at 107, 220 and 295 K, are shown

in Figure 9. These spectra are typical of superoxo-Ti(IV) anion radical species Ti($O_2^{\bullet-}$) [37]. Previous spectral simulations [34,36] have revealed three types of Ti(IV)-superoxo radical species (A, B and C) in TS-1, which are shown in Scheme 1 . These species differ mainly in the values of their g_z parameter, whereas g_x and g_y are almost the same for the three species. According to this, the spectra presented in Figure 9 show mainly the B-type species which is evidenced by its value of $g_z \approx 2.02$ obtained from the graph [34,36]. Moreover, as it was mentioned, such species can be associated with framework Ti(IV) sites. Therefore, the EPR spectra of our Ti-MCM-41 sample allow us to confirm the presence of Ti ions in tetrahedral isolated sites inside framework evidenced by DRUV-Vis and XPS.

On the other hand, it is known that the intensity of EPR signals depends on the population difference (n) of the two spin quantized energy levels (Ms= ±½). According to the Boltzmann function, the population difference is given by the following expression [38]:

$$n = N*tg(\Delta E/2kT) \qquad (1)$$

where N is the total number of spins, k is Boltzmann´s constant, T is the absolute temperature, and ΔE is the energy separation between the two spin quantized energy levels. If $\Delta E/2kT < 1$ [19] then the population difference can be rewritten as:

$$n \approx (N/2)(\Delta E/kT) \qquad (2)$$

Hence, the intensity of the EPR signal varies linearly with 1/T.

The intensity of the EPR signal of g_z parameter for our Ti-MCM-41 sample was graphed in terms of 1/T in the Figure 10 and the Equation (2) could be corroborated.

4. Conclusions

Ti-MCM-41 type molecular sieves with various compositions have been successfully prepared by hydrotermal synthesis at 373 K and compared to pure siliceous

MCM-41. The influence of various parameters such as Ti loading, nature of surfactant and synthesis time on the textural and structural properties was systematically studied. Besides the modification of the structural parameter a_0, it is probable that the nature of the surfactant used as a template affect to the cooperative character of the electrostatic S^+I^- assembly mechanism and consequently the structural regularity of the material. The incorporation of titanium to the silica structure was successfully achieved through 1 day of hydrothermal synthesis. Moreover, the MCM-41 material allowed the incorporation of different quantities of Ti (between 0.35 and 2.5 wt.%) without collapsing the structure. All the samples showed an ordered porous structure, high surface areas and a narrow mesopores size distribution. However, an incorporation of metal above 1 % affected both the degree of structural ordering and the values of surface area as well as the shape of the N_2 adsorption isotherm. N_2 adsorption and TEM studies of the samples with the highest Ti contents revealed the presence of large irregular cavities that permeate the entire bulk of the particles, in addition to the conventional mesopores present in MCM-41 type mesoporous materials. The existence of such secondary cavities might have relevance for catalysis, as it would probably enhance the diffusion of reagents through the particles. Ti was incorporated into the silica framework mainly in tetrahedral isolated sites, which was confirmed by DRUVA-Vis and XPS. In addition, superoxo-Ti(IV) species were identified over the catalyst surface after its contact with H_2O_2, and associated to the presence of tetrahedral titanium species in framework positions.

Acknowledgements

G. A. E. and M. K. S. CONICET Researchers; C. M. Ch. CONICET Doctoral Fellowship. This work was supported by the CONICET, the UTN-FRC and the UNSL of Argentina. The authors thank to A. Vallone, G. Amaya y M. Amaral (LaCSuMP-

UNSL, San Luis, Argentina) for their help in recording N_2 adsorption data, Dra. Teresa Causa (C.A.B. - Bariloche - Argentina) for their help in recording EPR data, Dra Isabel Díaz (ICP - Madrid - España) for their help in recording the TEM images and Dr J.L. García Fierro (ICP - Madrid - España) for their help in recording the XPS spectra.

References

[1] J. Thomas, Angew. Chem. Int. Ed. Engl., 33 (1994) 913.

[2] C. Kresge, M. Leonowicz, W. Roth, J. Vartuli, J. Beck, Nature, 359 (1992) 710.

[3] J. Vartuli, K. Schmidt, C. Kresge, W. Roth, M. Leonowicz, S. McCullen, S. Hellring, J. Beck, J. Schlenker, D. Olson, E. Sheppard, Chem. Mater., 6 (1994) 2317.

[4] J. Beck, C. Chu, I. Jonson, C. Kresge, M. Leonowicz, W. Roth, J. Vartuli, WO 91/11390 (1991).

[5] B. Chakraborty, B. Viswanathan, Catal. Today, 49 (1999) 253.

[6] A. Sayari, M. Jaroniec, T. Pinnavaia (Eds), Nanoporous Materials II, Stud. Surf. Sci. Catal., 2000, chap. 129.

[7] A. Sayari, M. Jaroniec (Eds), Nanoporous Materials III, Stud. Surf. Sci. Catal., 2002, chap. 129.

[8] A. Corma, Chem. Rev., 97 (1997) 2373.

[9] D. Serrano, J. Aguado, J. Escola, Ind. Eng. Chem. Res., 39 (2000) 1177.

[10] A. Ghanbari-Siahkali, A. Philippou, J. Dwyer, M. Anderson, Appl. Catal. A: Gen., 192 (2000) 57.

[11] J. Clark, Green Chem., 1 (1999) 1.

[12] K. Reddy, C. Song, Catal. Today, 31 (1996) 137.

[13] D. Trong On, D. Desplantrier-Giscard, C. Danumah, S. Kaliaguine, Appl. Catal., 222 (2001) 299.

[14] C. Berlini, M. Guidotti, G. Moretti, R. Psaro, N. Ravasio, Catal. Today, 60 (2000) 219.

[15] C. Berlini, G. Ferraris, M. Guidotti, G. Moretti, R. Psaro, N. Ravasio, Microp. Mes. Mat., 44-45 (2001) 595.

[16] J. Gallo, I. Paulino, U. Schuchardt, Appl. Catal. A: Gen, 266 (2004) 223.

[17] M.Guidotti, N. Ravasio, R. Psaro, G. Ferraris, G. Moretti, J. Catal, 214 (2003) 242.

[18] G. Eimer, S. Casuscelli, G. Ghione, M. Crivello, E. Herrero, Appl. Catal. A: Gen., 298 (2006) 232.

[19] S. Gregg, K. Sing, Adsorption Surface Area and Porosity, Academic Press, 1982.

[20] V. Rajakovic, S. Mintova, J. Senker, T. Bein, Mat. Sci. Eng. C, 23 (2003) 817.

[21] A. Sinha, S. Seelan, T. Akita, S. Tsubota, M. Haruta, Appl. Catal. A: Gen., 240 (2003) 243.

[22] M. Kruk, M. Jaroniec, Chem. Mater. 11 (1999) 2568.

[23] M. Kruk, M. Jaroniec, Y. Sakamoto, O. Terasaki, R. Ryoo, C. Ko, J. Phys. Chem. B 104 (2000) 292.

[24] I. Díaz, J. Pérez-Pariente, Chem. Mater. 14 (2002) 4641.

[25] D. Efremov, V. Fenelonov, Stud. Surf. Sci Catal., 62 (1991) 62.

[26] W. Zhang, M. Froba, J. Wang, P. Tanev, J. Wong, T. Pinnavaia, J. Am. Chem. Soc., 118 (1996) 9164.

[27] J. Choi, D.Kim, S. Chang, W. Ahn, Appl. Catal. A: Gen. 254 (2003) 225.

[28] D. Trong On, M. Kapoor, P. Joshi, L. Bonneviot, S. Kaliaguine, Catal. Lett. 44 (1997) 171.

[29] D. Trong On, S. Nguyen, V. Hulea, E. Dumitriu, S. Kaliaguine, Micropor. Mesopor. Mat. 57 (2003) 169.

[30] I. Grohmann, W. Pitz, G. Walther, H. Kosslick, V.A. Tuan, Surf. Interface Anal., 22 (1994) 403.

[31] S Contarini, P.A.W.Van der Heide, A.M. Prakash, L. J. Kevan, Electron Relat. Phenom., 125 (2002) 25.

[32] G. Moretti, A. Salvi, M. Guascito, F. Langerame, Surf. Interface Anal., 36 (2004) 1402.

[33] R. Bal, K. Chaudhari, D. Srinivas, S. Sivasanker, P. Ratnasamy, J. Mol. Catal. A: Chem., 162 (2000) 199.

[34] K. Chaudhari, D. Srinivas, P. Ratnasamy, J. Catal., 203 (2001) 25.

[35] V. Shetti, P. Manikandan, D. Srinivas, P. Ratnasamy, J. Catal., 216 (2003) 461.

[36] D. Sirinivas, P. Manikandan, S. Laha, R. Kumar, P. Ratnasamy, J. Catal., 217 (2003) 160.

[37] M. Anpo, N. Aikawa, Y. Kubokawa, M. Che, C. Louis and E. Giamello, J. Phis. Chem, 89 (1985) 5689.

[38] H. Box, Electron Paramagnetic Resonance Spectroscopy, Academic Press, New York, 1997.

Table 1: Physicochemical properties of the MCM-41 samples synthesized with different Ti contents and DTMABr as template, synthesis time = 1 day, 373 K.

Samples	Si/Ti [a]	Ti content [b] (wt.%)	a_0 (Å)	d_{DFT} [c] (Å)	V_p [d] (cm^3/g)	V_p (cm^3/g) [e] $0.4 < p/p_0 < 0.6$	Surface area [f] (m^2/g)
Ti-MCM-41(20)	20	2.50	37.2	27.39	0.830	0.25	1440
Ti-MCM-41(60)	60	1.12	36.4	27.25	0.7278	0.13	1649
Ti-MCM-41(180)	180	0.35	36.0	25.39	0.7833	0.05	1700
Si-MCM-41	∞	0.00	36.0	25.19	0.659	0.03	1790

[a] in synthesis gel; [b] in final solid product; [c]Pore diameter corresponding to the maximum of the pore size distribution obtained by the DFT method; [d]Total pore volume; [e] Pore volume associated with the hysteresis loop; [f] BET specific surface area

Scheme 1. Tentative structures of Ti(IV) species after the interaction with H_2O_2 (S: solvent).

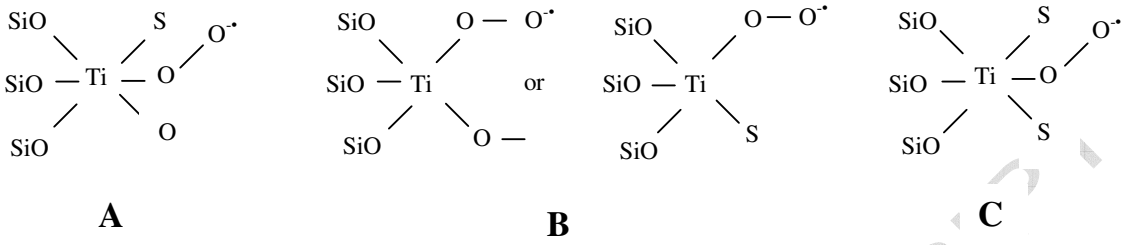

A **B** **C**

Figure captions

Figure 1: XRD patterns of Ti-MCM-41 prepared with (a) DTMABr and (b) CTMABr as templates. Si/Ti molar ratio = 60, synthesis time = 3 days, 373 K.

Figure 2: Effect of synthesis time on the degree of Ti-MCM-41 structural regularity. Si/Ti molar ratio = 60, DTMABr as template, 373 K.

Figure 3: XRD patterns of MCM-41 samples synthesized with different Ti contents and DTMABr as template, synthesis time = 1 day, 373 K. (a)Si-MCM-41, (b)Ti-MCM-41(180), (c)Ti-MCM-41(60), (d)Ti-MCM-41(20).

Figure 4: Nitrogen adsorption-desorption isotherms of the MCM-41 samples synthesized with different Ti contents and DTMABr as template, synthesis time = 1 day, 373 K.

Figure 5: DFT pore size distribution of the MCM-41 samples synthesized with different Ti contents and DTMABr as template, synthesis time = 1 day, 373 K.

Figure 6: TEM images at low (left) and high (right) magnification of Ti-MCM-41(20) sample.

Figure 7: DRUVA-Vis spectra of MCM-41 samples synthesized with different Ti contents and DTMABr as template, synthesis time = 1 day, 373 K. (a)Si-MCM-41, (b)Ti-MCM-41(180), (c)Ti-MCM-41(60), (d)Ti-MCM-41(20).

Figure 8: XPS in the Ti 2p region of Ti-MCM-41(20) sample.

Figure 9: EPR spectra of the superoxo-Ti(IV) species in Ti-MCM-41(20) after contact with aqueous H_2O_2 recorded at (a)107, (b)220 and (c)295 K.

Figure 10: EPR intensity variation of the superoxo-Ti(IV) species in Ti-MCM-41(20) as a function of temperature.

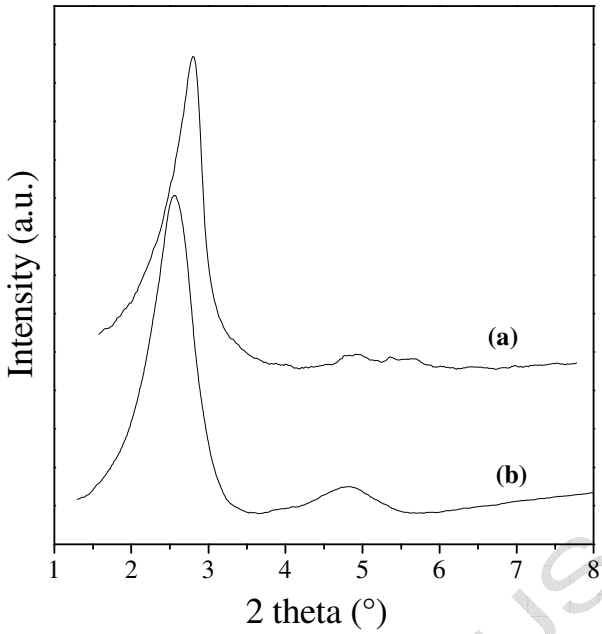

Figure 1

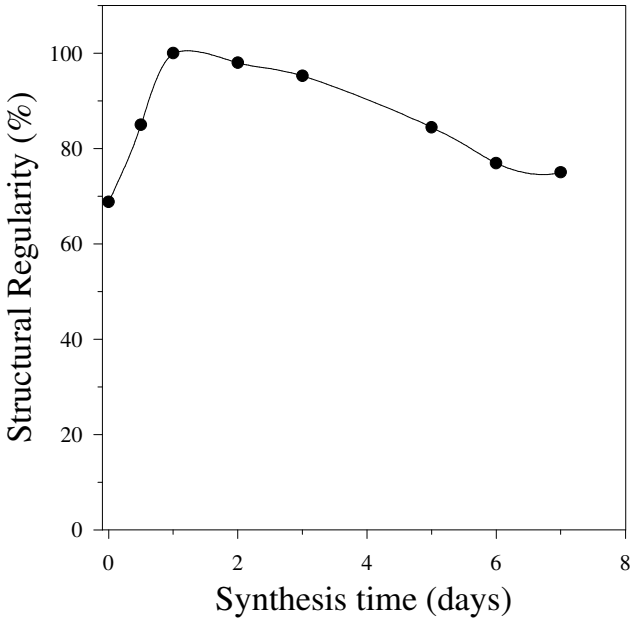

Figure 2

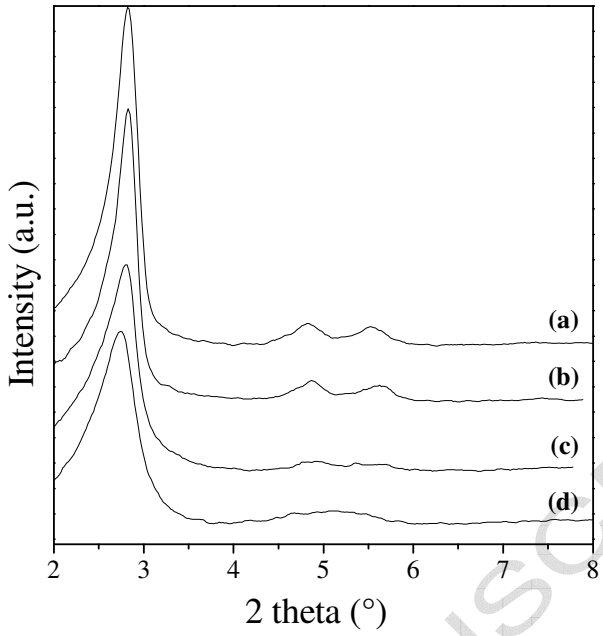

Figure 3

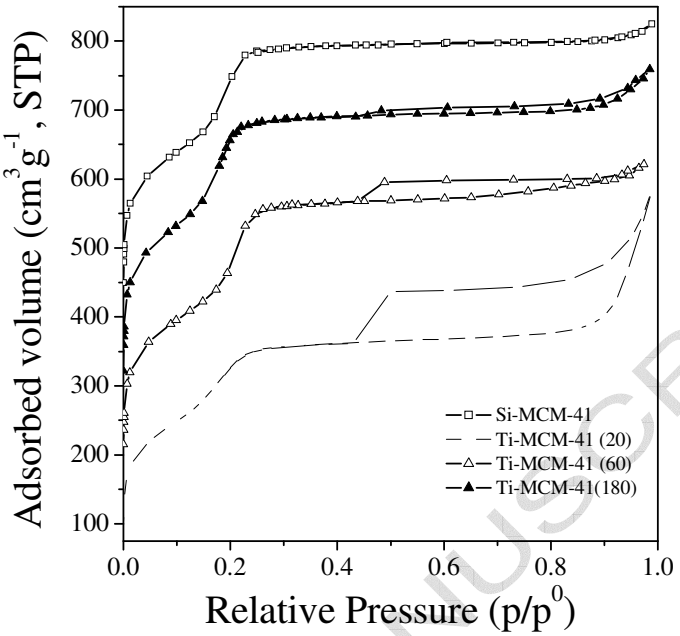

Figure 4

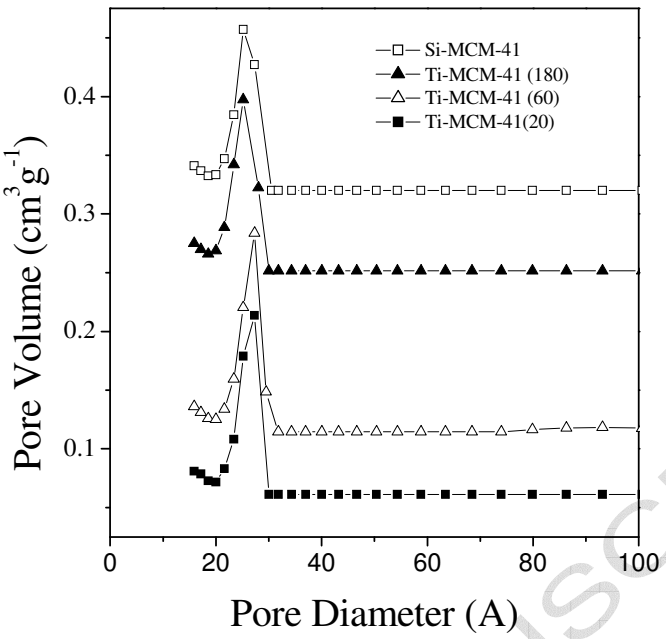

Figure 5

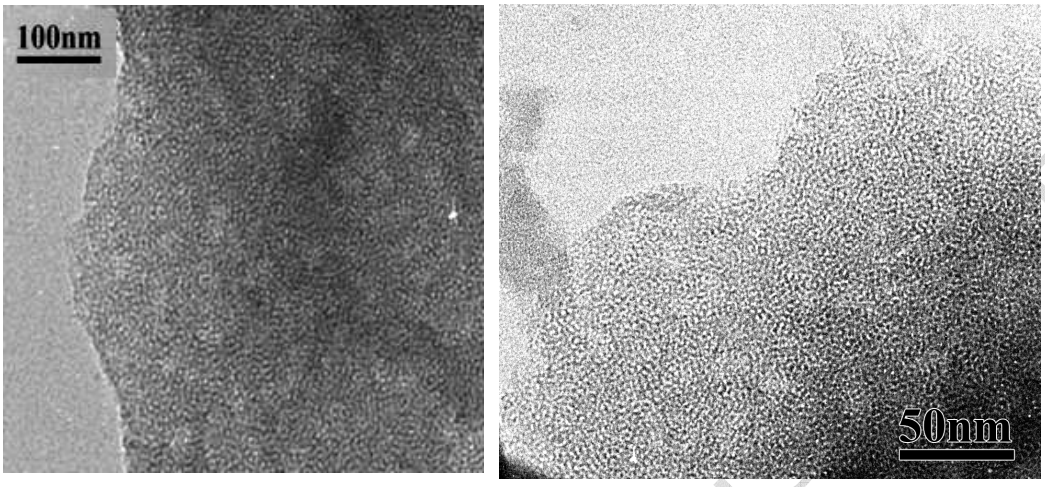

Figure 6

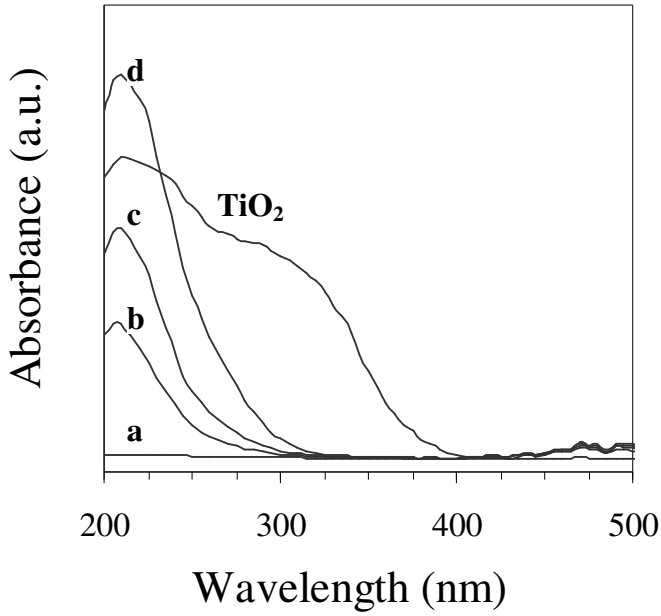

Figure 7

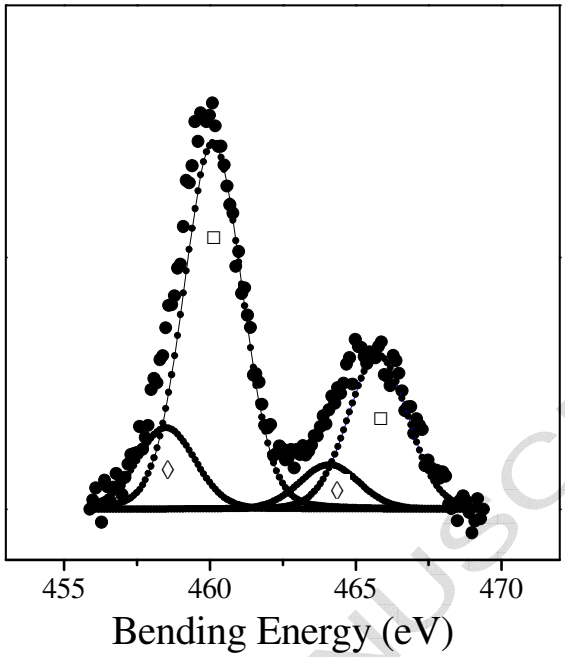

Figure 8

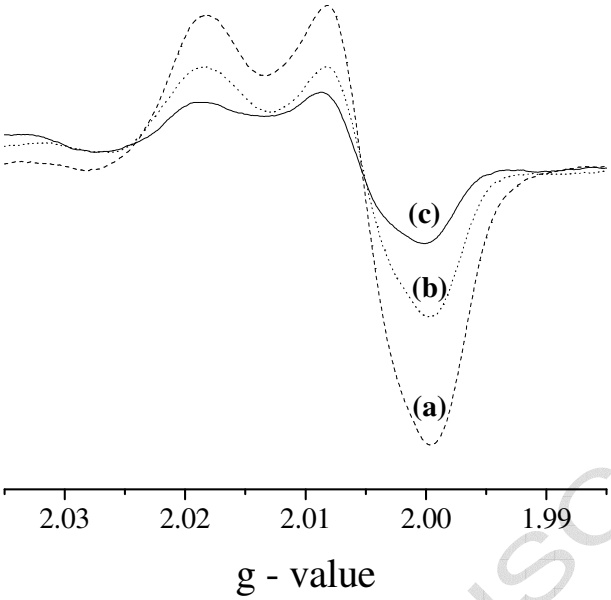

Figure 9

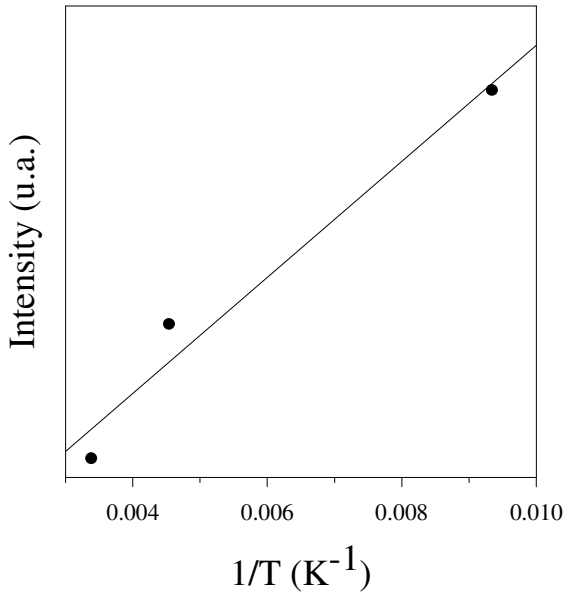

Figure 10